Published in final edited form as:
Neuroimage. 2010 November 1; 53(2): 553–564. doi:10.1016/j.neuroimage.2010.06.049.

Time lag dependent multimodal processing of concurrent fMRI and near-infrared spectroscopy (NIRS) data suggests a global circulatory origin for low-frequency oscillation signals in human brain

Yunjie Tong[1,2] and **Blaise deB. Frederick**[1,2,*]

[1] Brain Imaging Center, McLean Hospital, 115 Mill Street, Belmont, MA 02478, USA

[2] Consolidated Department of Psychiatry, Harvard Medical School, 25 Shattuck Ave., Boston, MA 02115, USA

Abstract

Low frequency oscillations (LFOs), characterized by frequencies in the range 0.01~0.1 Hz are commonly observed in blood-related brain functional measurements such as near-infrared spectroscopy (NIRS) and functional magnetic resonance imaging (fMRI). While their physiological origin and implications are not fully understood, these signals are believed to reflect some types of neuronal signaling, systemic hemodynamics, and/or cerebral vascular auto-regulation processes. Here, we examine a new method of integrated processing of concurrent NIRS and fMRI data collected on six human subjects during a whole brain resting state acquisition. The method combines the high spatial resolution offered by fMRI (~3 mm) and the high temporal resolution offered by NIRS (~ 80 ms) to allow for the quantitative assessment of temporal relationships between the LFOs observed at different spatial locations in fMRI data. This temporal relationship allowed us to infer that the origin of a large proportion of the LFOs is independent of the baseline neural activity. The spatio-temporal pattern of LFOs detected by NIRS and fMRI evolves temporally through the brain in a way that resembles cerebral blood flow dynamics. Our results suggest that a major component of the LFOs arise from fluctuations in the blood flow and hemoglobin oxygenation at a global circulatory system level.

Keywords

Low frequency oscillation; near-infrared spectroscopy; functional magnetic resonance imaging; functional connectivity; resting state

Introduction

Near-infrared spectroscopy (NIRS) is a non-invasive, low-cost functional brain imaging modality that measures hemoglobin concentration and oxygenation at high temporal resolution (~10 ms) in the cerebral cortex. Like other blood-related brain functional measurements, the NIRS signal is frequently dominated by low-frequency oscillations

*Corresponding author. Brain Imaging Center, McLean Hospital, 115 Mill Street, Belmont, MA 02478. Telephone: 1 (617) 855-3708 Fax: 1 (617) 855-2770 bbfrederick@mclean.harvard.edu.

(LFOs; typically defined as frequencies between 0.01 and 0.1 Hz (Zuo et al., 2010)), especially when signals associated with brain activation tasks are relatively small (Mayhew et al., 1996; Obrig et al., 2000; Tachtsidis et al., 2004; Zhang et al., 2005). In task activation studies, the LFO is typically reduced by averaging the response of many repetitions of a stimulus, and/or by high pass filtering. The physiological origins of this signal are hard to assess by NIRS alone due to the limitations of NIRS in terms of both penetration depth, which is limited to about 1–2 cm (thus allowing for sensitivity only to superficial cortical areas), and spatial resolution (~1 cm).

Likewise, LFOs are commonly observed in blood oxygenation level dependant (BOLD) fMRI, both during studies of task activation and resting-state activity (Arfanakis et al., 2000; Auer, 2008; Glover et al., 2000; Greicius and Menon, 2004; Gusnard and Raichle, 2001). The source of these oscillations has been attributed to some combination of resting state neural activity, “physiological noise” arising from fluctuations in blood oxygenation and flow arising from cardiac and blood pressure changes, respiratory effects that are secondary to the physiological effects of chest wall motion, etc, and “scanner noise”, a non specific term typically applied to 1/f signals that arise from machine instabilities. In fact, some “physiological noise” has been observed in water phantoms (Zarahn et al., 1997), which clearly represents instrument-related noise.

The detection and characterization of resting state networks of BOLD activity as measured with BOLD fMRI has been an extremely active area of study in the last few years (Biswal et al., 1995; Damoiseaux et al., 2006; Fox et al., 2005; Greicius et al., 2003). However, the origin and function of these networks is still controversial and a number of lines of evidence suggest that neuronal activation (Buzsaki and Draguhn, 2004) within resting state networks does not fully account for low frequency BOLD fluctuations in the brain. There appear to be global oscillations that are not attributable to a single network (Fox et al., 2009). Some studies suggest that the origins of these low frequency signals are predominantly vascular and do not directly represent neuronal signaling (Bhattacharyya and Lowe, 2004; Fukunaga et al., 2008). Some groups argue that this vascular signal is the result of global signals driven by the heartbeat, respiration and arterial blood pressure (Birn et al., 2006; Fukunaga et al., 2008; Glover et al., 2000; Wise et al., 2004), while others suggest the origin may lie in the regulation of regional cerebral blood flow (Katura et al., 2006). It is likely that there are both neural and vascular components to the low frequency oscillations in the brain. A recent study of concurrent fMRI and electroencephalographic recording suggested LFO reflects cyclic modulation of gross cortical excitability and long distance neuronal synchronization (Balduzzi et al., 2008; Buzsaki and Draguhn, 2004).

Several works have been published about concurrent fMRI-fNIRS studies in human volunteers during task activations (Huppert et al., 2006; Sassaroli et al., 2006; Strangman et al., 2002; Toronov et al., 2001). The focus of the majority of these studies was to validate the model that links the hemoglobin concentration changes (detected by NIRS) with the changes in the BOLD signal, by exploring the temporal correlations between the NIRS and the BOLD signal. In general, the reports found good correlations between BOLD and NIRS. Among them, Strangman et al. observed a slightly better correlation between BOLD signal and changes in oxyhemoglobin concentration (Δ[HbO]) (Strangman et al., 2002), while other group found good correlations between BOLD and changes in deoxyhemoglobin concentration (Δ[Hb]) ((Huppert et al., 2006; Toronov et al., 2003). So far, very few studies have been done on the resting state studies using both modalities simultaneously (Greve et al., 2009).

In the present study, we combined the high temporal resolution of NIRS (80 ms) with the high spatial resolution of fMRI (3.5 × 3.5 × 4 mm) to investigate the physiological origin of

LFOs detected by both modalities during the resting state. The goals of this resting state study were: 1) to examine the temporal and spatial characteristics of LFOs as measured with NIRS; 2) to determine the spatial extent of NIRS LFO in brain; and 3) to investigate temporal changes in the spatial patterns of LFO signal (identified by NIRS) throughout the brain in the BOLD data.

Because both NIRS and BOLD signals are sensitive to blood-oxygenation-related changes in the brain and both are able to accurately sample the low frequency band (< 0.1 Hz), we posit that there should be a strong temporal correlation between measurements of low-frequency physiological processes obtained using both techniques simultaneously. Conversely, these two imaging methods have completely different physical and instrumentation bases, so that we expect no correlation of instrumentation noise or image artifacts in the two imaging modalities. The correlated components of NIRS and BOLD datasets should only be related to biological/physiological signals from the tissue under study. This suggests that a novel integrated multi-modality processing strategy that offers the opportunity to characterize low-frequency physiological signals without contamination from instrumental noise and artifacts may offer new insights into the origin of the LFOs.

While previous studies have compared the results of simultaneously acquired NIRS and BOLD data, for the most part, the modalities have been considered independently. A counterexample is the work of Greve, et al (Greve et al., 2009) performing a synthesized processing of the NIRS and BOLD data. In this work, the NIRS signal was used as a regressor for BOLD analysis, as a method of characterizing (and removing) BOLD noise. The strategy of combined processing holds great potential for deriving information not possible using either modality alone. In the present study, we have extended this concept of simultaneous processing of NIRS and BOLD fMRI by additionally considering the effect of time delay on the correlation between the two modalities.

We will use the time course of the measured NIRS LFO signal (reference signal) from a cortical region as a regressor in a general linear model (GLM) analysis of the concurrently acquired fMRI dataset. The high spatial resolution and full brain coverage of fMRI offers an opportunity to examine how well the NIRS signal correlates with BOLD data not only in the region covered by both modalities, but throughout the brain. In this manner, all voxels in which BOLD activation is correlated with LFO measured by NIRS can be visualized. The BOLD voxels that have a high temporal correlation with the NIRS reference signal provide an indication of the spatial extent and location of the brain areas associated with NIRS LFO signal, and may provide insight into the physiological, hemodynamic, and/or functional source of the NIRS signal. By also considering the effect of time delay on the degree of correlation between the modalities, we also determined how these correlations change in time, and the spatial pattern of this change.

We applied this method in the present series of six case studies using healthy volunteers, and found that the NIRS signal is a sensitive probe for analyzing LFOs that are observed in BOLD data, as has been seen previously. We performed an analysis of simultaneously acquired NIRS and BOLD-fMRI data and found that the BOLD data shows significant correlations to the LFOs as modeled by the NIRS waveform (in widespread areas throughout the brain). Furthermore, by applying a range of time shifts (both advancing and delaying the timing) to the NIRS reference signal, we observed that the BOLD-measured LFOs evolve temporally through the brain in a manner that suggests a hemodynamic rather than neuronal origin, and a global rather than regional character.

Protocol

Concurrent NIRS and fMRI resting state studies were conducted on six healthy volunteers during a resting state acquisition (4M,2F, aged 28.0±4.69 y.o.). Informed consent was obtained prior to scanning. The protocol was approved by the Institutional Review Board at McLean Hospital and all volunteers read and signed an informed consent form prior to participating in this study. During the experiment, the participants were asked to lie quietly in the scanner with their eyes open while fMRI and NIRS data were recorded. During this time, the subject viewed a gray screen with a central fixation point.

fMRI acquisition and physiological monitoring

All MR data were acquired on a Siemens TIM Trio 3T scanner (Siemens Medical Systems, Malvern, PA) using a 12-channel phased array head matrix coil. A high-resolution anatomic image set was acquired for slice positioning and coregistration of the functional data (T1 weighted multiecho MP-RAGE3D (van der Kouwe et al., 2008)), resolution (RL, AP, SI) of 1.33 × 1 × 1 mm, TI = 1,100 ms, TR/TE1, TE2 = 2530/3.31,11.61 ms, FOV = 171 × 256 × 256 mm, 128 × 256 × 256 pixels, 2x GRAPPA, total imaging time 4 min 32 sec). This was followed by the resting state scan (2 dummy shots, 260 time points, TR/TE=1500/30 ms, flip angle 75 degrees, matrix = 64 × 64 on a 220 × 220 mm FOV, 29 3.5 mm slices with 0.5 mm gap parallel to the AC-PC line extending down from the top of the brain, GRAPPA acceleration factor of 3). Physiological waveforms (pulse oximetry, and respiratory depth) were recorded using the scanner's built-in wireless finger-tip pulse oximeter and respiratory belt. After the completion of the fMRI acquisition, 3D velocity encoded phase contrast images were acquired to map the blood vessels in the head (1 slab, aligned with the AC-PC plane, 160 0.9mm slices/slab, 0.8×0.8mm resolution in the readout (AP, FOV=200mm) and phase encode (RL, FOV=150mm) directions, velocity encoding 30cm/s, total acquisition time 5:55).

NIRS acquisition

An MRI compatible NIRS probe, with three collection and two illumination optical fibers, with source-detector distances of 1 or 3 cm (see Figure 1), was placed over the right prefrontal area of each participant (roughly between Fp1 and F7 in the 10–20 system) and held in place by an elastic band around the head. The position of the probe was chosen due to its easy accessibility (no hair) and relatively short distance from the scalp to the cortex (11–13 mm on average) in this area (Okamoto et al., 2004). The probe had embedded MRI visible markers to identify the probe location on the anatomic MRI images (Figure 1). Each illumination fiber delivered light from two laser diodes emitting at wavelengths of 690 and 830 nm. The laser diodes and three optical detectors (photomultipliers tubes, Hamamatsu Photonics R928) were housed in a near-infrared tissue imager (Imagent, ISS, Inc., Champaign, IL), which was placed in the MRI control room. The two more medial optical paths, with probe spacings of 1 and 3 cm, are labeled B1 and C1 respectively, and the more lateral 3 cm path is labeled D2. The two optical collection points, which were 3 cm away from their corresponding laser sources, are labeled C and D; the detector 1 cm away is labeled B. The optical probe and the Imagent instrument were connected by 10 m long optical fibers. The sampling rate of NIRS data acquisition was 12.5 Hz. fMRI data was collected for 6 minutes 30 seconds; NIRS data was recorded continuously during this time as well as for several minutes before and after the fMRI acquisition.

Each pair of raw NIRS time courses (690 and 830 nm data) were converted into two time courses representing temporal changes of the concentrations of oxy-hemoglobin and deoxy-hemoglobin according to the differential path length factor method (Matcher, 1994) using a Matlab program (The Mathworks, Natick, MA). The time courses of Δ[HbO] and Δ[Hb]

measured with NIRS were then anti-aliased and down-sampled to the fMRI acquisition frequency of 0.67 Hz (1/1.5 s). Figures 2(a) and 2(d) show the temporal traces of Δ[HbO] and Δ[Hb] measured from path C1 on subject 3 and the corresponding resampled data. The down-sampled Δ[HbO] data, as well as the down-sampled Δ[Hb] data were later used as regressors in the general linear model (GLM) analysis of the BOLD data. In order to account for any possible time misalignment between the NIRS and BOLD data, we also applied a range of time shifts to the NIRS signal prior to resampling. A positive time shift value means that the resampled waveform corresponds to events that happened prior to the time the NIRS data was recorded. We considered 21 time shift values covering the range of −7.2 s to +7.2 s with respect to the unshifted signal. We did not expect any significant correlation with regressors shifted outside of this range. Each of these time series was down-sampled to 260 data points. Figure 2(c) and 2(f) shows the 21 regressors with 0.72 s time shift between the consecutive ones.

NIRS and fMRI data analysis

For each subject, both NIRS and fMRI data were analyzed using FEAT, part of the FSL analysis package (FMRIB Expert Analysis Tool, v5.98, http://www.fmrib.ox.ac.uk/fsl, Oxford University, UK) (Smith et al., 2004)). fMRI preprocessing steps included motion correction (Jenkinson and Smith, 2001), slice time correction, spatial smoothing (Gaussian kernel of full-width-half-maximum = 5 mm) and high pass temporal filtering (cut-off frequency = 0.02 Hz to remove very slow instrumental drifts).

The only regressor of interest used in these analyses was the Δ[HbO] obtained from NIRS data collected from path C1 (Figure 1) at one of the time lags described above to model the global physiological signal (LFO) observed in BOLD. Since the Δ[HbO] represents a real-time measurement of hemodynamics, neither the temporal derivative nor a hemodynamic response function were used. The temporal high pass filter (0.02 Hz) was applied to the regressor for consistency. The motion parameters, estimated from the motion correction preprocessing step on the fMRI data, were included as confounds to further remove motion-correlated noise.

The GLM was calculated voxel by voxel using FMRIB's improved linear model (FILM) with prewhitening (Woolrich et al., 2001). Regression coefficients at each voxel were transformed to z statistics indicating the statistical significance of model-related BOLD signal change. The significance threshold at the voxel level was set as $z > 2.3$. A cluster threshold of $p < 0.05$ was applied to the clusters which survived the local voxel threshold, and the significance of the cluster was computed. The fMRI data were coregistered to the subject's structural scan, and then to the standard MNI152 brain (Evans, 1993).

This image analysis was repeated 21 times for each of the time shifted copies of the NIRS Δ[HbO] regressor. The resulting thresholded z-statistic maps were concatenated in time and displayed in sequence as a movie in order to assess the spatial pattern of Δ[HbO]-correlated regions as they changed over time.

The same procedure was applied to the NIRS −Δ[Hb] regressor. Since the BOLD signal is negatively correlated with Δ[Hb] (as opposed to positively correlated with Δ[HbO]), the sign of the regressor is inverted to allow direct comparison of the two analyses.

A total of 42 analyses (21 for Δ[HbO] regressors and 21 for −Δ[Hb] regressors) were carried out for the data collected over each path (C1, B1 and D2), then the whole procedure was repeated for each subject. The results of the Δ[HbO] and Δ[Hb] obtained from C1 on subject 3 are discussed in detail, while only the results of the Δ[HbO] (from path C1) are shown for the rest of the subjects.

Results and Discussion

Characteristics of the NIRS signal

The Δ[HbO] and Δ[Hb] collected from path C1 on subject 3 will be discussed in detail due to its high signal to noise ratio and no visible motion artifacts. In Figure 2, the time traces of Δ[HbO] and Δ[Hb] and their resampled versions are shown. Figure 2(a), (b) and (c), shows the time traces of Δ[HbO], its enlarged section, and the 21 regressors of various time shifts (separated by 0.72 s) used in the study. Figure 2(d), (e) and (f) show the corresponding graphs for Δ[Hb].

Cerebral blood has a high oxygen saturation, varying from almost 100% in arterial blood to ~60% in venous blood, and a resulting high ratio of [HbO] to [Hb]. Figure 2 indicates that the Δ[HbO] signal amplitude (and signal to noise ratio (SNR)) is approximately 3–4 times the size of the Δ[Hb] (as seen in Figure 2(b) and 2(e)). As result, Δ[HbO] is chosen to be the regressor discussed in detail below. The time trace of resampled Δ[Hb] is negatively correlated with that of Δ[HbO] (as seen in Figure 2(c) and 2(f)). Therefore, −Δ[Hb] was used as regressors to generate positive correlations in order to compare with the results from Δ[HbO].

In order to fully understand the main components of the NIRS LFO signal, we performed a Fourier analysis of the temporal traces of Δ[HbO] and the other physiological recordings, including the peripheral pulse signal measured by the finger-tip oximeter and the respiration measured by the breathing belt. The graphs on the left panel of Figure 3 show the power spectra of the Δ[HbO] measured with NIRS over path C1, the peripheral pulse measured with pulse oximeter, and the respiratory belt waveform of each subject, while the graphs on the right panel are the enlarged view of the frequency spectrum (up to 0.4 Hz) for Δ[HbO] and its resampled version (after high pass filtering by FEAT at 0.2 Hz).

Figure 3 shows a number of results: 1) the cardiac frequencies, as indicated by the data from both the oximeter and NIRS, were centered around 1.0 Hz for most of the subjects, except subject 6, whose heart rate was around 0.7 Hz. The cardiac frequency is a prominent component of the NIRS signal in all subjects. 2) The respiration frequencies, derived from the breathing belt data, center between 0.2 to 0.4 Hz. In subjects 1 and 3, a double-peak respiration frequency was observed. The respiration frequencies are strong components of the NIRS data in subject 1 and 3, but not in the other subjects. Even in subjects 1 and 3, the signals at the breathing frequency are much smaller than those at either the cardiac frequencies or in the low frequency band. The direct effect of the respiratory waveform on the NIRS data (i.e. at the fundamental respiratory frequency) is relatively small and variable. It should be noted that this does not preclude the possibility that subtle changes in the breathing rate or depth of inhalation might affect the data outside of this band (as found by others (Birn et al., 2006)) – these effects would likely be part of the LFO signal, and through-space susceptibility effects at the breathing frequencies can affect the fMRI data without affecting the NIRS signal. 3) The LFOs, at frequencies around and below 0.1 Hz, were prominent in the NIRS data and not observed in either the pulse oximeter or respiratory belt data (although this may be in part due to high pass filtering within the physiological recording system). The graphs on the right panel of Figure 3 show that the NIRS data after lowpass filtering and resampling retains only the frequencies < 0.35 Hz. The dominant components are below 0.1 Hz. The fMRI data analysis revealed a spatially complex and widespread pattern of voxels (including distinct, bilaterally symmetric clusters) with time courses significantly correlated with the Δ[HbO] regressor.

Voxels where BOLD signals correlate with time-shifted Δ[HbO]

Twenty one z-statistic maps of BOLD fMRI signals were calculated, where NIRS-measured Δ[HbO] traces (shifted from −7.2 to 7.2 s in increments of 0.72 s), were used as regressors for every subject (the same procedure was applied using the −Δ[Hb] data). Figure 4 displays 21 z-statistic maps with increments of 0.72 s using Δ[HbO] as regressors for subject 3. The number on the top left of each graph indicates the time-shift of the regressor for that particular graph. Each z-statistic map was the result of an independent GLM analysis using a different regressor. This is possible because the NIRS recording was longer than the fMRI time series in both directions, and the NIRS signal has temporal resolution as high as 80 ms (acquisition rate of 12.5 Hz), so that we could choose steps as small as 80 ms. However, because the TR is 1.5 s, a time step of 0.72 s was sufficient to adequately sample the subtle details of the signal changes over time.

In Figure 4, the z-statistic maps of activation to the various shifted Δ[HbO] regressors show areas where the BOLD signal is significantly positively correlated with Δ[HbO]. The axial level of the brain was chosen to be at the position that one of the two NIRS probe markers (the one between source 1 and detector D; refer to Figure 1) was visible (circled in red in the z-statistic map of no time shift). Instead of being only concentrated underneath the marker (a reasonable expectation as NIRS is known to only sample tissue depths of 1–2 cm below the optical probe,), the voxels with time courses modeled by the Δ[HbO] activations are widespread, at a range of depths, and bilaterally symmetrical. As noted above, by performing multiple GLM analyses of the BOLD data using a population of NIRS regressors that have been shifted in time, time-dependent changes in the spatial patterns of significantly NIRS-correlated BOLD signal can be observed throughout the brain (Figure 4). From the sagittal view of the z-maps, the BOLD signal wave starts to appear at locations near the callosomarginal, frontopolar and parietooccipital arteries. As time progresses, the wave becomes widespread in the gray matter, as it passes through capillary beds and then retreats towards the venous systems through several paths, including: 1) the superior cerebral vein to the superior sagittal sinus (also visible from the coronal view); 2) the inferior sagittal sinus combining internal cerebral vein to the straight sinus; 3) through the transverse sinus (visible in the coronal view); 4) through the anterior and posterior spinal veins. The path the wave follows through the brain strongly resembles that of the cerebral vasculature.

The total time span of the wave's passage through the brain from appearance to disappearance was about 9.36 s (−5.04 ~ 4.32 s) in Subject 3 as seen in Figure 4. However, the maxima of the z values in a given voxel as a function of time lag are quite broad. A more accurate measure of the relative delay of the wave between two voxels can be derived by comparing the time lag of the peak z-value in each voxel. Figure 5 shows the position of two voxels in (a) and their z-value vs. time shift in (b). In this analysis, a higher resolution of 0.24 s was used in the time shift dimension (from −7.2 – 7.2 s) resulting in 61 z values. Both voxels are on the superior sagittal sinus. According to Figure 5(b), the relative times for the peak of the wave to reach the purple circle and green circle are −0.24 s and 1.44 s respectively, therefore the time it took the wave to travel from the purple circle to the green is about 1.68 s. This method was then applied to two activated voxels, which appeared at the beginning (t=−5.04 s) and the end (t=4.32 s) of the wave's observed passage through the brain, in order to estimate the time for the wave to pass the whole brain. Figure 5(c) shows the position of these two voxels and their time of appearance. Figure 5(d) shows their z-value vs. time shift. The time for the wave to pass the brain is about 6.48 s, which is consistent with the literature (Crandell et al., 1973). We acknowledge that this is an unsophisticated calculation, which does not take into account the fact that the fMRI voxels are likely to contain blood in multiple compartments.

We also observed that the z-values were highest in the venous system (especially superior sagittal sinus and transverse sinus), which is likely due to the fact that these vessels are considerably larger than other brain blood vessels. To further demonstrate this point, a higher threshold of z>4 was applied to the concatenated z-statistic maps in Figure 4, and the maximum value along the time lag dimension was selected for each voxel to generate a 3-D map, which was then surface rendered using fslview (part of the FSL package). Figure 6 shows the result of this combined z-statistic map in a 3-D rendition in 6(c) using fslview, together with the 3-D rendering images of the structure brain in 6(a) and that of phase contrast angiogram in 6(b) using OsiriX (Rosset et al., 2004). By comparing 6(b) and 6(c), one can identify the superficial cerebral veins, the superior sagittal sinus, and the transverse sinus. Figures of the arterial and venous organization of the cerebral vasculature can be found in the literature, for example in Chaper 6 of “Functional Magnetic Resonance Imaging” (Huettel et al., 2009).

Voxels where BOLD signals correlate with time-shifted −Δ[Hb]

Figure 7 displays 21 z-statistic maps with increments of 0.72 s using −Δ[Hb] as regressors for subject 3. The results depict similar patterns of activation in each z-statistic map and similar passage of the wave though the brain, when compared to the result of Δ[HbO]. This is unsurprising, given the high correlation (correlation=0.64) between resampled Δ[HbO] and −Δ[Hb]. However, the activation maps of −Δ[Hb] have smaller spatial extent. This is likely due to lower the SNR of the −Δ[Hb] measurement compared to Δ[HbO], which results in lower z-values, and fewer voxels exceeding the threshold of 2.3.

Multisubject analysis

To show that this phenomenon is repeatable, comparable z-statistic maps are presented for all 6 subjects in Figure 8 and 9 (sagittal and axial views respectively). The sagittal slice was chosen at midline of the brain and the axial slice parallel to the AC-PC plane was chosen at lateral ventricles for all the subjects. Each row of Figure 8 and 9 represents the data from one subject, and shows thresholded z-statistic maps of BOLD fMRI signals using Δ[HbO] as regressors over the range of time lag values, with a time shift interval of 0.72 s. Figure 8 and 9 show a number of effects: 1) the spatial evolution of the activation pattern throughout the brain is similar in all subjects, with the strongest activations observed in the draining vein system, including superior sagittal sinus, straight sinus, internal sagittal vein; 2) the timecourse of pattern evolution varies significantly from subject to subject. The time difference between the z-value peaks in the first and last voxels where activation was observed in each brain (i.e. repetition of the calculation depicted in Figure 5(c) for subject 3) reveals the average time it took the wave traveling through the brain is 6.08s (ranging from 4.08 – 6.96 s). This indicates that the time taken for the LFO to pass the brain is subject-specific. 3) There are differences of the spatial pattern between subjects. For example, the pattern observed in subject 6 is less prominent than in the other subjects. This may be due to improper NIRS probe coupling to the brain (perhaps due to poor probe placement), differences in the subject’s vasculature, or some other variation in subject physiology (the subject has an extremely low resting heart rate of 48 beats per minute).

The fact that the set of voxels where the BOLD signal correlates with the NIRS-detected LFOs evolves temporally through the brain indicates that a major component of the LFOs is widely spatially distributed throughout the brain, and this distribution alters over time, which is not consistent with a regional vascular origin. Moreover, the temporal evolution of the LFOs appears to closely follow the cerebral circulatory system from arteries to the gray matter (where most blood vessels reside), to the venous system, which is not consistent with a neural origin. The component of the LFOs that moves with the blood is already present

before the blood reaches gray matter (as seen by the prominent activation at positive time shifts). This suggests a source outside of the brain.

If the LFO signal is moving with the blood, and is not of neural origin, it is presumably due to extracerebral sources, such as cardiac and respiratory fluctuations. This view is supported by the literature. Katura, et al (Katura et al., 2006) performed a detailed information transfer analysis on NIRS LFO data collected in the sensorimotor region, and determined that approximately 35% of the HbO signal could be attributed to external cardiac factors (20% from heart rate (HR), 5% from arterial blood pressure (ABP), and 10% from ABP × HR.) The remaining 65% of the signal was attributed to “other factors”, which they postulated were primarily due to “respiration or regional cerebral hemodynamics and metabolism”. In fact, Birn has shown (Birn et al., 2006; Birn et al., 2009) that accounting for respiratory factors, particularly the respiration volume per time (RVT), removes a significant proportion of the global low frequency BOLD noise variance (RVT alone removed 75% as much noise variance on average as RETROICOR correction, which generates regressors based on the cardiac and respiratory waveforms (Glover et al., 2000)). Although Birn’s methodology and imaging modality were different from Katura’s, it is not unreasonable to assume that directly considering respiratory factors would significantly increase the proportion of the LFO signal that is attributable to extracerebral circulatory factors.

This observation is not inconsistent with the existence of widespread networks of low frequency BOLD oscillations in the brain arising from neural connectivity (Zuo et al., 2010). There is overwhelming evidence that these networks exist and are related to cognition (Fox and Raichle, 2007). The present study supports the notion that a significant portion of the signal in this frequency range arises from a different source and that this signal confounds the detection of resting-state connectivity networks. The method described in this report offers the potential to fit and remove this blood-borne noise component and may greatly improve the efficiency of detection of resting-state neural activation.

Spatial variation of NIRS data

In the previous analysis, the NIRS signal obtained from path C1 was the focus. The signals from paths D2 and B1 are highly correlated with that of path C1. This is reflected in the high average correlation coefficients between the Δ[HbO] of paths B1 and C1, B1 and D2, and C1 and D2 for all subjects (0.91, 0.85 and 0.93). The correlation coefficients between data from C1 and D2 are the highest; this mainly because 1) the two paths are only 1.2 cm from each other; 2) the source-detector distance for detector C1 and D2 are the same (3.0 cm, see Figure 1). Therefore the areas probed by each detector are largely overlapped. The source-detector distance for path B1 is only 1.0 cm (see Figure 1); this would limit the NIRS to be sensitive only to the superficial layer (skin and scalp) (Patterson and Pogue, 1994). The high correlation between B1 and C1 (D2) indicate that the main source of the signal detected over these paths is the same. However, we cannot determine whether the source is in the superficial layer or the deeper layer. The z-statistic maps of activation to the various shifted Δ[HbO] regressors obtained from detector B1 show the similar patterns as to the various shifted Δ[HbO] regressors obtained from detector paths C1 and D2. This is consistent with the argument that the NIRS signal detected over these paths originate from the vessel-rich cortex, however, it could be that the blood vessels in the skin and scalp (directly underneath the probe), which experienced the same LFO as majority of vessels in the brain, are the main sources. Further studies are required to resolve the issue, for instance, by using a pair of source and detector whose distance is even smaller than 1.0 cm, or to position the probe over a sinus, so the brain will not be visible, to be sure of detecting only the superficial layer and compare the result with the signal from other detectors (with bigger source-detector distance).

Conclusions

The present report describes an integrated processing method for concurrently collected NIRS and fMRI data, which was used to evaluate the data collected on 6 human participants during resting state scans. The method is similar to the seed voxel technique used to explore connectivity in BOLD datasets, but in this case, the “seed timecourse” was measured from outside the brain with a different modality. The high temporal resolution offered by NIRS means that the “seed” we chose can provide dynamic temporal information to reveal temporal as well as spatial connectivity. NIRS data is a valuable tool to enhance the utility of fMRI data, especially in the study of LFOs.

The present study also demonstrated that LFOs are prominent in all of the NIRS channels, and identified that a high correlation exists both between NIRS channels and with the BOLD signal over a widely distributed set of voxels. The spatial pattern and temporal evolution of the pattern formed by these voxels resembles the circulatory system in the brain. Further analyses using the shifted LFOs regressor revealed that the pattern propagates through the circulatory system over the course of about 6–7 seconds, consistent with the signal being carried by flowing blood.

These findings imply that a major component of the LFOs detected by both NIRS and fMRI arises from the propagation of endogenous global blood flow and oxygenation fluctuations through the cerebral vasculature, rather than from local variations in neuronal activation (i.e. not related to the task or resting state connectivity) or localized cerebral blood flow changes.

Previous work by Greve, (Greve et al., 2009) has shown that the unshifted NIRS signal can be used to denoise fMRI data. We propose that by determining the optimal regressor time shift on a per voxel basis (i.e. the time shift that provides the maximum correlation with the noise regressor, as performed above), the degree of noise reduction is likely to be significantly improved. Further work in this area is necessary to determine the most efficient method for implementing this procedure.

More interesting is the possibility that multimodal NIRS/fMRI correlation time shift imaging may provide a novel contrast mechanism that can be exploited as a tool for characterizing cerebral blood flow directly. The data in this study indicates that blood in arterial, venous, and capillary compartments all show detectable signals, and time shifts between various regions are easily determined. Further optimization of the technique may allow quantitation of other blood flow parameters. This is particularly attractive as there is no requirement for special MR acquisition parameters (other than a somewhat shorter TR than is typical for resting state studies) or exogenous contrast agents, so this information can be extracted from typical fMRI datasets without imposing major restrictions on experiment design.

Acknowledgments

The authors thank Angelo Sassaroli and Sergio Fantini for their comments and suggestions in the development of this analysis method. This work was supported by the National Institutes of Health, Grant No. R21-DA021817.

References

Arfanakis K, Cordes D, Haughton VM, Moritz CH, Quigley MA, Meyerand ME. Combining independent component analysis and correlation analysis to probe interregional connectivity in fMRI task activation datasets. Magn Reson Imaging. 2000; 18:921–930. [PubMed: 11121694]

Auer DP. Spontaneous low-frequency blood oxygenation level-dependent fluctuations and functional connectivity analysis of the 'resting' brain. Magn Reson Imaging. 2008; 26:1055–1064. [PubMed: 18657923]

Balduzzi D, Riedner BA, Tononi G. A BOLD window into brain waves. Proc Natl Acad Sci U S A. 2008; 105:15641–15642. [PubMed: 18843102]

Bhattacharyya PK, Lowe MJ. Cardiac-induced physiologic noise in tissue is a direct observation of cardiac-induced fluctuations. Magn Reson Imaging. 2004; 22:9–13. [PubMed: 14972388]

Birn RM, Diamond JB, Smith MA, Bandettini PA. Separating respiratory-variation-related fluctuations from neuronal-activity-related fluctuations in fMRI. Neuroimage. 2006; 31:1536–1548. [PubMed: 16632379]

Birn RM, Murphy K, Handwerker DA, Bandettini PA. fMRI in the presence of task-correlated breathing variations. Neuroimage. 2009; 47:1092–1104. [PubMed: 19460443]

Biswal B, Yetkin FZ, Haughton VM, Hyde JS. Functional connectivity in the motor cortex of resting human brain using echo-planar MRI. Magn Reson Med. 1995; 34:537–541. [PubMed: 8524021]

Buzsaki G, Draguhn A. Neuronal oscillations in cortical networks. Science. 2004; 304:1926–1929. [PubMed: 15218136]

Crandell D, Moinuddin M, Fields M, Friedman BI, Robertson J. Cerebral transit time of 99m technetium sodium pertechnetate before and after cerebral arteriography. J Neurosurg. 1973; 38:545–547. [PubMed: 4711624]

Damoiseaux JS, Rombouts SA, Barkhof F, Scheltens P, Stam CJ, Smith SM, Beckmann CF. Consistent resting-state networks across healthy subjects. Proc Natl Acad Sci U S A. 2006; 103:13848–13853. [PubMed: 16945915]

Evans, AC.; Collins, DL.; Mills, SR.; Brown, ED.; Kelly, RL.; Peters, TM. 3D statistical neuroanatomical models from 305 MRI volumes. IEEE-Nuclear Science Symposium and Medical Imaging Conference; 1993. p. 1813-1817.

Fox MD, Raichle ME. Spontaneous fluctuations in brain activity observed with functional magnetic resonance imaging. Nat Rev Neurosci. 2007; 8:700–711. [PubMed: 17704812]

Fox MD, Snyder AZ, Vincent JL, Corbetta M, Van Essen DC, Raichle ME. The human brain is intrinsically organized into dynamic, anticorrelated functional networks. Proc Natl Acad Sci U S A. 2005; 102:9673–9678. [PubMed: 15976020]

Fox MD, Zhang D, Snyder AZ, Raichle ME. The global signal and observed anticorrelated resting state brain networks. J Neurophysiol. 2009; 101:3270–3283. [PubMed: 19339462]

Fukunaga M, Horovitz SG, de Zwart JA, van Gelderen P, Balkin TJ, Braun AR, Duyn JH. Metabolic origin of BOLD signal fluctuations in the absence of stimuli. J Cereb Blood Flow Metab. 2008; 28:1377–1387. [PubMed: 18382468]

Glover GH, Li TQ, Ress D. Image-based method for retrospective correction of physiological motion effects in fMRI: RETROICOR. Magn Reson Med. 2000; 44:162–167. [PubMed: 10893535]

Greicius MD, Krasnow B, Reiss AL, Menon V. Functional connectivity in the resting brain: a network analysis of the default mode hypothesis. Proc Natl Acad Sci U S A. 2003; 100:253–258. [PubMed: 12506194]

Greicius MD, Menon V. Default-mode activity during a passive sensory task: uncoupled from deactivation but impacting activation. J Cogn Neurosci. 2004; 16:1484–1492. [PubMed: 15601513]

Greve, DN.; Goldenholz, D.; Kaskhedikar, G.; JRP; Moran, L.; Schwartz, CE.; Fischl, B.; Wald, LL.; Rosen, B.; Triantafyllou, C.; Boas, DA. BOLD Physiological Noise Reduction using Spatio-Spectral-Temporal Correlations with NIRS ISMRM. Hawaii: 2009.

Gusnard DA, Raichle ME. Searching for a baseline: functional imaging and the resting human brain. Nat Rev Neurosci. 2001; 2:685–694. [PubMed: 11584306]

Huettel, SA.; Song, AW.; McCarthy, G. Chapter 6: From Neuronal to Hemodynamic Activity. Functional Magnetic Resonance Imaging. Sinauer Associates, Inc; Sunderland, MA: 2009. p. 172-173.

Huppert TJ, Hoge RD, Diamond SG, Franceschini MA, Boas DA. A temporal comparison of BOLD, ASL, and NIRS hemodynamic responses to motor stimuli in adult humans. Neuroimage. 2006; 29:368–382. [PubMed: 16303317]

Jenkinson M, Smith S. A global optimisation method for robust affine registration of brain images. Med Image Anal. 2001; 5:143–156. [PubMed: 11516708]

Katura T, Tanaka N, Obata A, Sato H, Maki A. Quantitative evaluation of interrelations between spontaneous low-frequency oscillations in cerebral hemodynamics and systemic cardiovascular dynamics. Neuroimage. 2006; 31:1592–1600. [PubMed: 16549367]

Matcher SJ. Use of the water absorption spectrum to quantify tissue chromophore concentration changes in near-infrared spectroscopy. Physics in Medicine and Biology. 1994; 39:177–196. [PubMed: 7651995]

Mayhew JE, Askew S, Zheng Y, Porrill J, Westby GW, Redgrave P, Rector DM, Harper RM. Cerebral vasomotion: a 0.1-Hz oscillation in reflected light imaging of neural activity. Neuroimage. 1996; 4:183–193. [PubMed: 9345508]

Obrig H, Neufang M, Wenzel R, Kohl M, Steinbrink J, Einhaupl K, Villringer A. Spontaneous low frequency oscillations of cerebral hemodynamics and metabolism in human adults. Neuroimage. 2000; 12:623–639. [PubMed: 11112395]

Okamoto M, Dan H, Sakamoto K, Takeo K, Shimizu K, Kohno S, Oda I, Isobe S, Suzuki T, Kohyama K, Dan I. Three-dimensional probabilistic anatomical cranio-cerebral correlation via the international 10–20 system oriented for transcranial functional brain mapping. Neuroimage. 2004; 21:99–111. [PubMed: 14741647]

Patterson MS, Pogue BW. Mathematical model for time-resolved and frequency-domain fluorescence spectroscopy in biological tissues. Applied Optics. 1994; 33:1963–1974. [PubMed: 20885531]

Rosset A, Spadola l, Ratib O. OsiriX: An Open-Source Software for Navigating in Multidimensional DICOM Images. Journal of Digital Imaging. 2004; 17:205–216. [PubMed: 15534753]

Sassaroli A, de BFB, Tong Y, Renshaw PF, Fantini S. Spatially weighted BOLD signal for comparison of functional magnetic resonance imaging and near-infrared imaging of the brain. Neuroimage. 2006; 33:505–514. [PubMed: 16945553]

Smith SM, Jenkinson M, Woolrich MW, Beckmann CF, Behrens TE, Johansen-Berg H, Bannister PR, De Luca M, Drobnjak I, Flitney DE, Niazy RK, Saunders J, Vickers J, Zhang Y, De Stefano N, Brady JM, Matthews PM. Advances in functional and structural MR image analysis and implementation as FSL. Neuroimage. 2004; 23(Suppl 1):S208–219. [PubMed: 15501092]

Strangman G, Culver JP, Thompson JH, Boas DA. A quantitative comparison of simultaneous BOLD fMRI and NIRS recordings during functional brain activation. Neuroimage. 2002; 17:719–731. [PubMed: 12377147]

Tachtsidis I, Elwell CE, Leung TS, Lee CW, Smith M, Delpy DT. Investigation of cerebral haemodynamics by near-infrared spectroscopy in young healthy volunteers reveals posture-dependent spontaneous oscillations. Physiol Meas. 2004; 25:437–445. [PubMed: 15132309]

Toronov V, Walker S, Gupta R, Choi JH, Gratton E, Hueber D, Webb A. The roles of changes in deoxyhemoglobin concentration and regional cerebral blood volume in the fMRI BOLD signal. Neuroimage. 2003; 19:1521–1531. [PubMed: 12948708]

Toronov V, Webb A, Choi JH, Wolf M, Michalos A, Gratton E, Hueber D. Investigation of human brain hemodynamics by simultaneous near-infrared spectroscopy and functional magnetic resonance imaging. Med Phys. 2001; 28:521–527. [PubMed: 11339749]

van der Kouwe AJ, Benner T, Salat DH, Fischl B. Brain morphometry with multiecho MPRAGE. Neuroimage. 2008; 40:559–569. [PubMed: 18242102]

Wise RG, Ide K, Poulin MJ, Tracey I. Resting fluctuations in arterial carbon dioxide induce significant low frequency variations in BOLD signal. Neuroimage. 2004; 21:1652–1664. [PubMed: 15050588]

Woolrich MW, Ripley BD, Brady M, Smith SM. Temporal autocorrelation in univariate linear modeling of FMRI data. Neuroimage. 2001; 14:1370–1386. [PubMed: 11707093]

Zarahn E, Aguirre GK, D'Esposito M. Empirical analyses of BOLD fMRI statistics. I. Spatially unsmoothed data collected under null-hypothesis conditions. Neuroimage. 1997; 5:179–197. [PubMed: 9345548]

Zhang Y, Brooks DH, Franceschini MA, Boas DA. Eigenvector-based spatial filtering for reduction of physiological interference in diffuse optical imaging. J Biomed Opt. 2005; 10:11014. [PubMed: 15847580]

Zuo XN, Di Martino A, Kelly C, Shehzad ZE, Gee DG, Klein DF, Castellanos FX, Biswal BB, Milham MP. The oscillating brain: complex and reliable. Neuroimage. 2010; 49:1432–1445. [PubMed: 19782143]

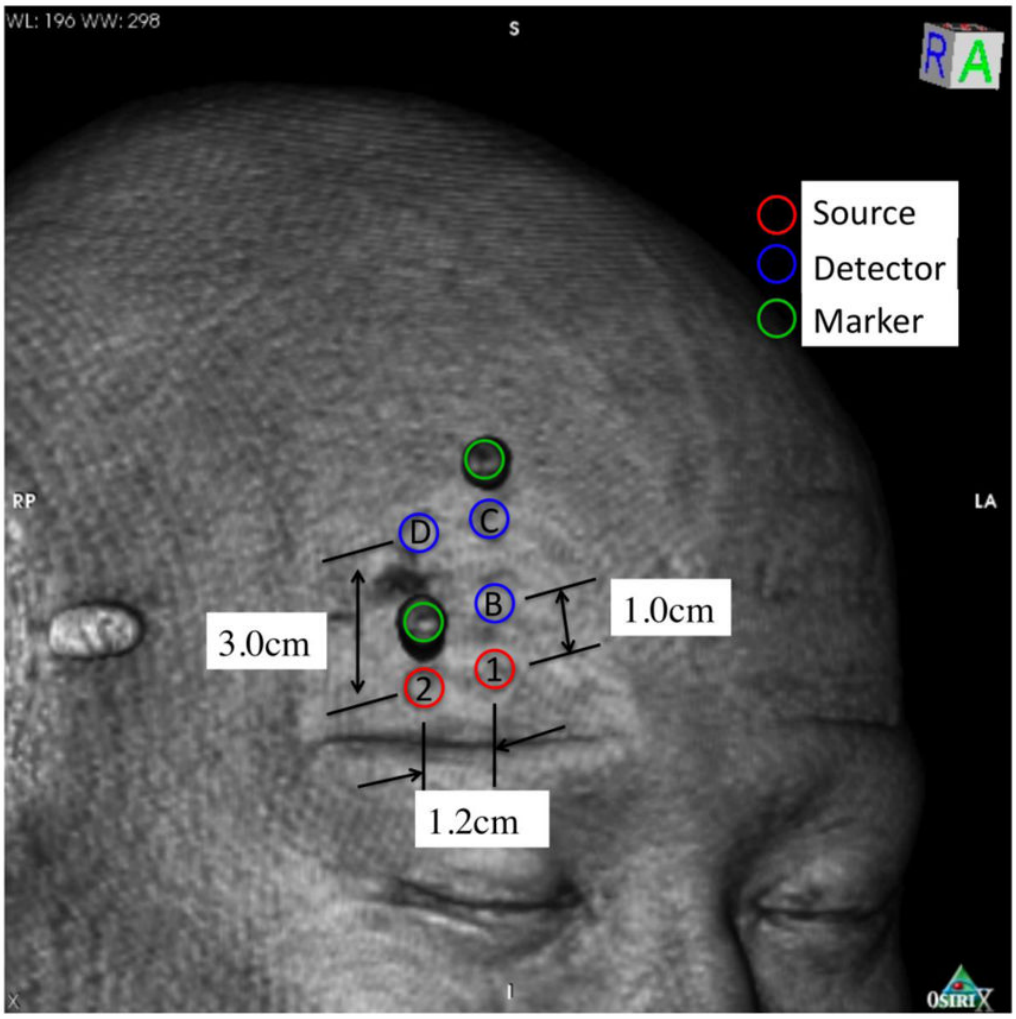

Figure 1.
3-D reconstructions of Subject 5's forehead from the structural scan using OsiriX (Rosset et al., 2004). The positions of the detectors and sources are clearly marked by the MR-visible markers and some imprints of the source and detector fibers. The distances between paired sources and detectors are 3 cm (C1 and D2) and 1 cm (B1).

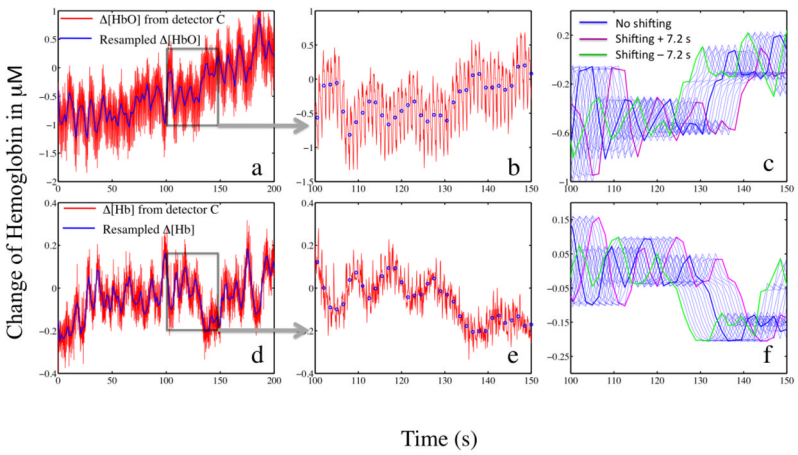

Figure 2.

Temporal trace of data collected over path C1 for Subject 3. (a) Original Δ[HbO] (blue) and its resampled data (red). (b) Enlarged section of original and resampled Δ[HbO] indicated by the black block in (a). (c) 21 regressors of various time shifting (separated by 0.72 s) used in the study from Δ[HbO]. (d), (e) and (f) are the corresponding graphs of (a), (b) and (c) with Δ[Hb] calculated from data collected over the same path.

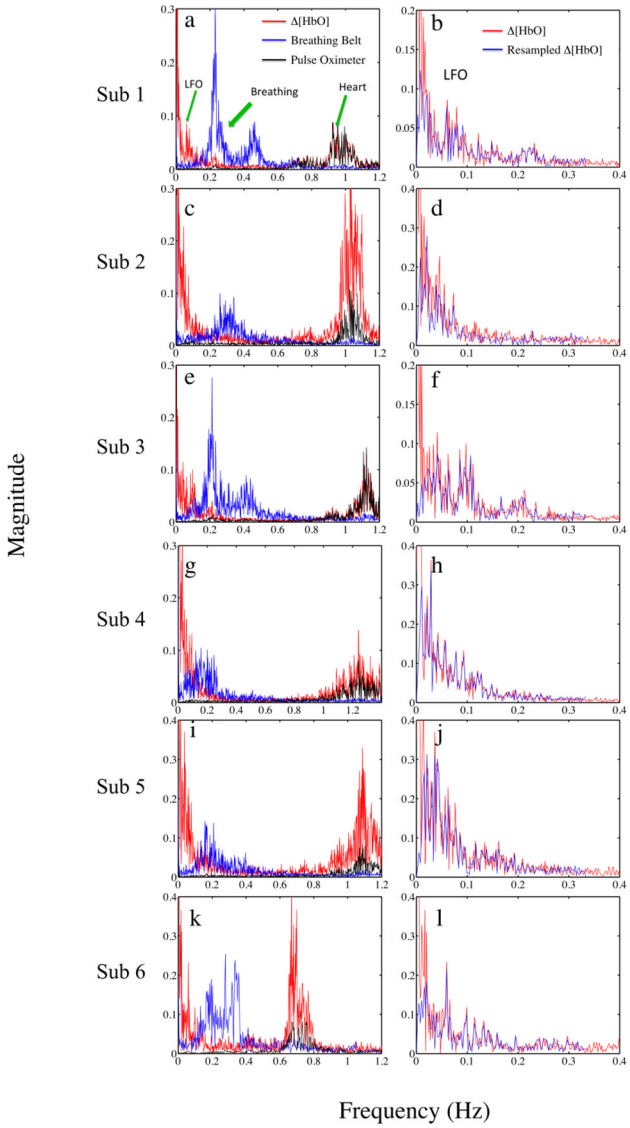

Figure 3.

The left panel (a, c, e, g, i, k) are the power spectra of Δ[HbO] (calculated from path C1), oxygenation and respiration waves obtained by the simultaneous recording of the subject during the experiment through the finger-tip oximeter and respiration belt for the subject 1–6. The right panel (b, d, f, h, j, l) are the corresponding spectra of Δ[HbO] for the subject 1–6, calculated from path C1 and their resampled data after high-pass filtered by FEAT at 0.2 Hz. Note after resampling, the main component of the signal is the LFO.

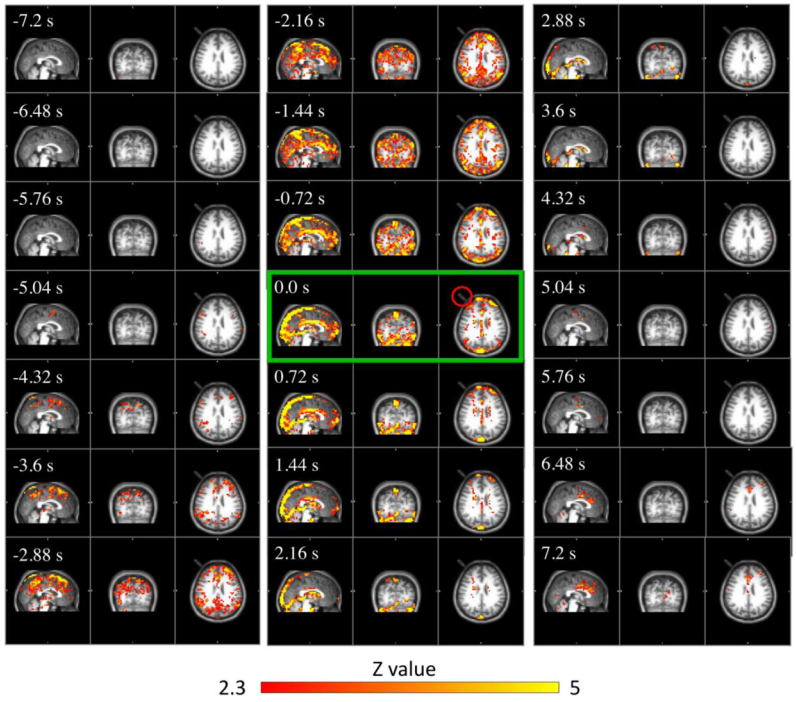

Figure 4.

z-statistic maps of the brain (subject 3) using NIRS Δ[HbO] (path C1) as regressors that shifted from −7.2 to 7.2 s seconds in 0.72 second steps. The number on the upper left corner of each graph indicates the regressor's time shift for that analysis. The z-statistic map with the green boundary is the map in which the NIRS regressor has not been shifted. The red circle calls out the position of one of the markers, which is closer to the source.

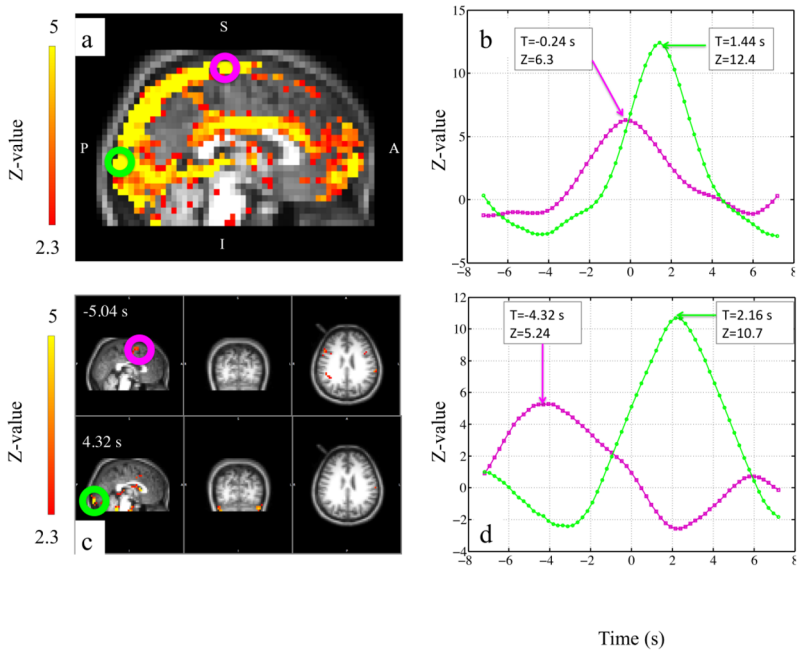

Figure 5.

Illustration of the procedure for calculating the travel time of the LFO from one voxel to the other. (a) Sagittal view of Subject 3 with z-statistic map at 0 time shift overlaid; two voxels on the superior sagittal sinus are chosen, as shown in purple and green circles. (b) plot of z-value vs. time shift for the two voxels in (a) with their maxima marked. (c) two z-statistic maps of different time shifts were picked from Figure 4 to select two voxels appeared at beginning and end of the wave's passage. (d) plot of z-value v.s. time shift for the two voxels in (c) with their maxima marked.

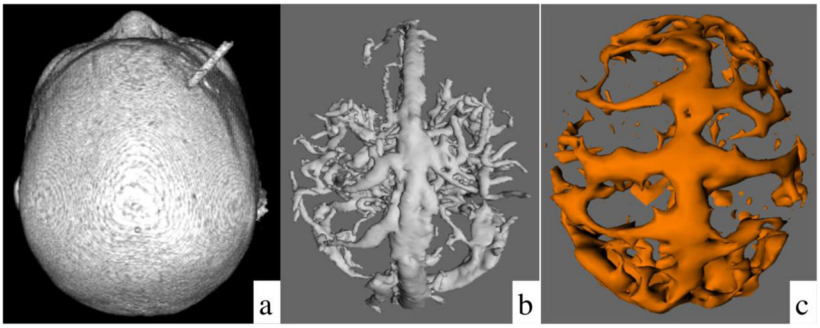

Figure 6.

Comparison of the 3-D rendered images of the subject 3's head using different methods. (a) 3-D rendering structural images of the subject 3's head with the markers on it. (b) 3-D reconstructions of phase contrast images showing the main blood vessels. (c) 3-D reconstructions using the maximum z-value over time lag maps of the NIRS Δ[HbO] ($z > 4$).

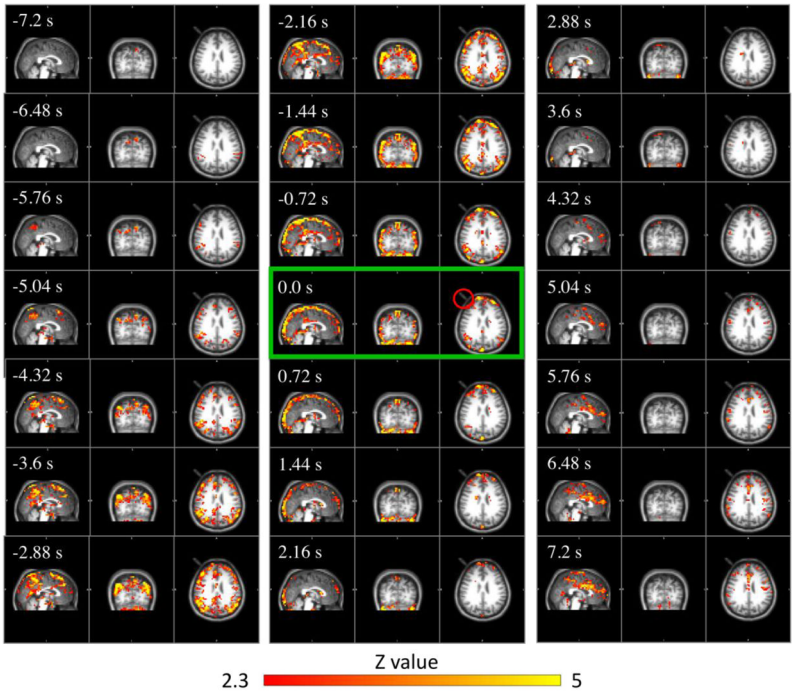

Figure 7.

z-statistic maps of the brain (Subject 3) using NIRS −Δ[Hb] (path C1) as shifted from −7.2 to 7.2 s seconds in 0.72 second steps. The number on the upper left corner of each graph indicates the regressor's time shift for that analysis. The z-statistic map with the green boundary is the map, in which the NIRS regressor has not been shifted. The red circle calls out the position of one of the markers, which is closer to the source.

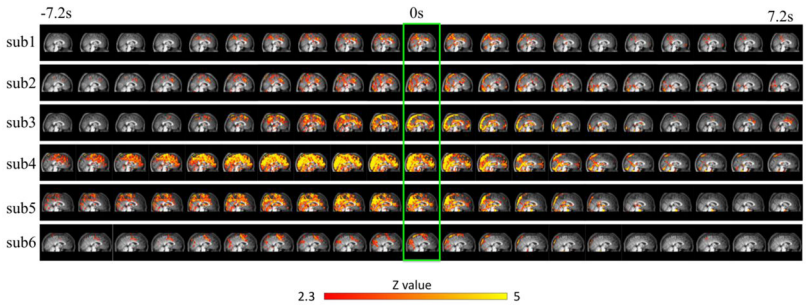

Figure 8.

z-statistic maps from a midline sagittal slice (Subjects 1–6), using NIRS Δ[HbO] (path C1) data as regressors shifted from −7.2 to 7.2 s seconds in 0.72 second steps. The z-statistic maps with the green boundaries are the maps, in which the NIRS regressor has not been shifted.

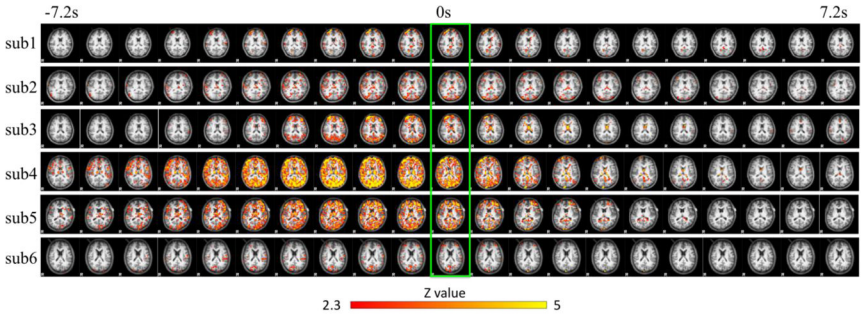

Figure 9.

z-statistic maps from an axial slice parallel to the AC-PC plane through the lateral ventricles (Subjects 1–6), using NIRS Δ[HbO] (path C1) data as regressors shifted from −7.2 to 7.2 s seconds in 0.72 second steps. The z-statistic maps with the green boundaries are the maps, in which the NIRS regressor has not been shifted.